

# The P2X7 receptor directly interacts with the NLRP3 inflammasome scaffold protein

Alessia Franceschini,\* Marina Capece,\* Paola Chiozzi,\* Simonetta Falzoni,\* Juana Maria Sanz,<sup>†</sup> Alba Clara Sarti,\* Massimo Bonora,\*<sup>‡</sup> Paolo Pinton,\*<sup>‡</sup> and Francesco Di Virgilio\*<sup>‡,1</sup>

\*Department of Morphology, Surgery and Experimental Medicine, Section of Pathology, Oncology and Experimental Biology, <sup>†</sup>Department of Medical Sciences, Section of Internal Medicine, Gerontology, and Clinical Nutrition, and <sup>‡</sup>Laboratory of Technologies for Advanced Therapies, University of Ferrara, Ferrara, Italy

**ABSTRACT** The P2X7 receptor (P2X7R) is a known and powerful activator of the NOD-like receptor (NLR)P3 inflammasome; however, the underlying pathways are poorly understood. Thus, we investigated the molecular mechanisms involved. The effect of P2X7R expression and activation on NLRP3 expression and recruitment was investigated by Western blot, RT-PCR, coimmunoprecipitation, and confocal microscopy in microglial mouse cell lines selected for reduced P2X7R expression and in primary cells from P2X7R<sup>-/-</sup> C57BL/6 mice. We show here that P2X7R activation by ATP (EC<sub>50</sub> = 1 mM) or benzoyl-ATP (EC<sub>50</sub> = 300 μM) and P2X7R down-modulation caused a 2- to 8-fold up-regulation of NLRP3 mRNA in mouse N13 microglial cells. Moreover, NLRP3 mRNA was also up-regulated in primary microglial and macrophage cells from P2X7R<sup>-/-</sup> mice. Confocal microscopy and immunoprecipitation assays showed that P2X7R and NLRP3 closely interacted at discrete subplasmalemmal sites. Finally, P2X7R stimulation caused a transient (3–4 min) cytoplasmic Ca<sup>2+</sup> increase localized to small (2–3 μm wide) discrete subplasmalemmal regions. The Ca<sup>2+</sup> increase drove P2X7R recruitment and a 4-fold increase in P2X7R/NLRP3 association within 1–2 min. These data show a close P2X7R and NLRP3 interaction and highlight the role of P2X7R in the localized cytoplasmic ion changes responsible for both NLRP3 recruitment and activation.—Franceschini, A., Capece, M., Chiozzi, P., Falzoni, S., Sanz, J. M., Sarti, A. C., Bonora, M., Pinton, P., and Di Virgilio, F. The P2X7 receptor directly interacts with the NLRP3 inflammasome scaffold protein. *FASEB J.* 29, 000–000 (2015). [www.fasebj.org](http://www.fasebj.org)

**Key Words:** purinergic receptors • extracellular ATP • inflammation

THE INFLAMMASOME IS A caspase-activating complex essential for processing and activation of the proinflammatory

Abbreviations: 3D, 3-dimensional; ASC, apoptosis-associated speck-like protein containing a CARD; ATPR, ATP-resistant clone; BzATP, 2'(3')-O-(4-benzoylbenzoyl)adenosine 5'-triphosphate; CTR, control; DAMPs, damage-associated-molecular patterns; GAPDH, glyceraldehyde 3-phosphate dehydrogenase; GFP, green fluorescent protein; NLR, NOD-like receptor; P2X7R, P2X7 receptor; shRNA, short hairpin RNA; TBS-T buffer, 10 mM Tris-HCl, 150 mM NaCl, pH 8.0, and 1% Tween-20; WT, wild-type

cytokines IL-1β and IL-18 (1, 2). This complex is formed by the assembly of 3 basic components: a scaffold protein belonging to the NOD-like receptor (NLR) family (with the exception of the AIM2 and pyrin inflammasomes), the adaptor protein apoptosis-associated speck-like protein containing a CARD (ASC), and procaspase-1 (3, 4). Depending on the scaffold protein, 10 different inflammasome subtypes are known, among which the NLRP3 inflammasome is the most commonly activated in immune cells in response to pathogen-associated molecular patterns (PAMPs) or damage-associated-molecular patterns (DAMPs) (5). The NLRP3 inflammasome is constitutively expressed in many cells, especially in immune cells, where it plays a central role in response to infections and in general in the pathogenesis of inflammation (5). The mechanism of activation of the NLRP3 inflammasome is as yet obscure. Although a direct NLRP3–PAMP interaction has been postulated, no strong proof for such a direct interaction has been thus far provided. Most recent evidence now points to an indirect mechanism based on the local decrease of the K<sup>+</sup> concentration (6, 7).

It has been known for several years that K<sup>+</sup> efflux is a very potent stimulus for caspase-1 activation and pro-IL-1β release, but it is unclear whether this is a generalized mechanism. Very recent data now provide robust evidence to support a key role of the K<sup>+</sup> drop in NLRP3 inflammasome activation by virtually all stimuli thus far tested (7). One of the most potent activators of the NLRP3 inflammasome is extracellular ATP acting at the P2X7 receptor (P2X7R). The P2X7R is ideal as a means to trigger a drop in the intracellular K<sup>+</sup> concentration because of its ability to activate an intrinsic (or associated) large conductance plasma membrane pore (8–10). However, even assuming that a K<sup>+</sup> drop is the (main) mechanism of P2X7R-NLRP3 inflammasome coupling, it is highly unlikely that K<sup>+</sup> depletion occurs in a delocalized fashion throughout the cytosol. On the contrary, it would be much more physiologic that the cytoplasmic ion change was restricted at

<sup>1</sup> Correspondence: Department of Morphology, Surgery and Experimental Medicine, Section of Pathology, Oncology and Experimental Biology, University of Ferrara, Via Borsari, 46, 44121 Ferrara, Italy. E-mail: [fdv@unife.it](mailto:fdv@unife.it)  
doi: 10.1096/fj.14-268714

This article includes supplemental data. Please visit <http://www.fasebj.org> to obtain this information.

specific sites, possibly where P2X7R and NLRP3 are in close proximity. For this reason, we explored the hypothesis that P2X7R and NLRP3 were localized in the vicinity of each other and might even directly interact at selected subplasmalemmal sites.

In the present work we show that P2X7R modulates NLRP3 expression at the mRNA and protein level; P2X7R and NLRP3 are coimmunoprecipitated in the same protein complex and colocalize to discrete cytoplasmic subplasmalemmal regions; and P2X7R activation drives P2X7R recruitment and enhances P2X7R/NLRP3 colocalization at sites of cytoplasmic Ca<sup>2+</sup> increase and K<sup>+</sup> drop. These observations clarify the mechanism of NLRP3 inflammasome activation in immune cells.

## MATERIALS AND METHODS

### Cell and peritoneal macrophage cultures

Microglial wild-type (WT; N13wt) and ATP-resistant (N13ATPR) N13 cells were obtained and cultured in RPMI 1640 medium (Sigma-Aldrich, St. Louis, MO, USA), supplemented with 10% heat-inactivated fetal bovine serum, 100 U/ml penicillin, and 100 µg/ml streptomycin (Euroclone, Milano, Italy) (11). B16 cells were grown in RPMI medium supplemented with 10% fetal bovine serum, 100 U/ml penicillin, 100 µg/ml streptomycin, and nonessential amino acids (Sigma-Aldrich). Cells were stimulated with ATP (for 5, 15, 30, and 60 minutes; 2 mM; Sigma-Aldrich), 2' (3')-O-(4-benzoylbenzoyl) adenosine 5'-triphosphate (BzATP; for 15 or 30 minutes; 300 µM; Sigma-Aldrich), and LPS (for 1 or 2 hours; 1 µg/ml, cat no. L6529, impurity < 3% protein; Sigma-Aldrich). B16 transfection was performed with TransIT-2020 transfection reagent (Tema Ricerca, Bologna, Italy) following the manufacturer's instructions. The P2X7 short hairpin RNA (shRNA) in pSuper.neo.green fluorescent protein (GFP) vector was a kind gift of Dr Diaz-Hernandez (Universidad Complutense, Madrid, Spain). Stably transfected cell lines were obtained by selection with G418 sulfate (0.2–0.8 mg/ml; Calbiochem, La Jolla, CA, USA). Single cell-derived clones (B16 shRNA) were obtained by limiting dilution. HEK293 ratP2X7-GFP cells (HEK293-P2X7R-GFP) were obtained and cultured as previously described by Lemaire *et al.* (12). Peritoneal macrophages were isolated from the peritoneal cavity of WT and P2X7<sup>-/-</sup> adult mice as previously described (12) and immediately processed for mRNA extraction and Western blot analysis. Primary mouse microglia cells were isolated from 2- to 4-day-old postnatal mice as described previously (13). All procedures were performed in accordance with the Italian institutional guidelines in compliance with national and international laws and policies.

### Immunofluorescence and confocal microscopy

For microscopy, cells were fixed with 4% paraformaldehyde/PBS for 10 minutes at room temperature, followed by a 45-minute incubation with blocking solution (5% bovine serum albumin, 5% fetal bovine serum, and 0.1% Triton-X 100). The following antibodies were used: polyclonal rabbit anti-mouse P2X7R (1:100 dilution; cat no. P8232; Sigma-Aldrich) and monoclonal rat anti-mouse NLRP3 (1:25 dilution, cat no. MAB 7578; R&D Systems, Minneapolis, MN, USA). The following secondary antibodies were used: donkey anti-rabbit AlexaFluor 594-conjugated (cat no. ab150064) and goat anti-rat AlexaFluor 488-conjugated (cat no. ab150157; 1:500 dilution; Abcam, Cambridge, United Kingdom). Cells were counterstained with DAPI (Fluoroshield Mounting Medium; Abcam). Control experiments were performed by staining cells only with secondary antibodies. Images

were visualized with a fluorescence microscope (DMI400B; Leica, Wetzlar, Germany) or with a confocal microscope (LSM 510; Zeiss, Oberkochen, Germany) and analyzed with ImageJ software (National Institutes of Health, Bethesda, MD, USA). Colocalization analysis was performed with the ImageJ plugin JACoP and Colocalization Colormap (14). P2X7R and NLRP3 relative gray values were quantified across the x-y axes of the cell body (indicated as yellow line in Figs. 4A and 5A, B) at a focal plane set at 3 µm. Three-dimensional (3D) reconstruction (Fig. 4D) and orthogonal views (Figs. 4C and 5E, F) were obtained with high-magnification confocal Z-stack (7 planes, 0.8 µm band-pass width) images (Zeiss) elaborated with ImageJ plugin JACoP. A total of 20 cells for each condition were analyzed.

### Immunoprecipitation

For coimmunoprecipitation experiments, cells were incubated on ice for 45 minutes in the following lysis buffer: 150 mM NaCl, 5 mM EDTA, 20 mM Tris, pH 7.5, 1% Triton X-100, 1 mM benzamide, 1 mM phenylmethylsulfonyl fluoride, and protease inhibitor cocktail (all from Sigma-Aldrich). Lysates were clarified by centrifugation for 5 minutes at 20,000 g before use. Total protein content of cell lysates was measured with the Bradford assay. Immunoprecipitation was performed using Dynabeads Protein A (Life Technologies, Carlsbad, CA, USA) according to the manufacturer's instructions. Dynabeads were preincubated with polyclonal rabbit anti-NLRP3 (cat no. ab91525; Abcam) and polyclonal rabbit anti-P2X7R (cat no. P8232; Sigma-Aldrich) antibodies before addition of lysates. As negative controls, eluates from antibody-coated beads in the absence of cell lysate and eluates from antibody-uncoated beads incubated together with the cell lysate were loaded (as shown in Fig. 4E, F).

### Immunoblots

Proteins were analyzed on Bolt Mini Gels 4–12% SDS-PAGE (Life Technologies) and transferred onto nitrocellulose paper (GE Healthcare Life Sciences, Milano, Italy). Membranes were blocked with 2% nonfat milk (Bio-Rad, Hercules, CA, USA) and 5% bovine serum albumin (Sigma-Aldrich) in TBS-T buffer (10 mM Tris-HCl, 150 mM NaCl, pH 8.0, and 1% Tween-20) and probed overnight at 4°C with rabbit anti-P2X7R (1:200 dilution; Sigma-Aldrich), rat anti-NLRP3 (1:250 dilution; R&D Systems), monoclonal mouse anti-ASC (1:2000 dilution, cat. no. 04147; Millipore, Billerica, MA, USA), or rabbit anti-actin (1:1000 dilution, cat. no. A2668; Sigma-Aldrich) antibodies. Membranes were washed 3 times for 5 min with TBS-T buffer and incubated in the same buffer for 2 hours at room temperature with horseradish peroxidase-conjugated secondary polyclonal antibody goat anti-mouse (1:500 dilution, cat no. ab97240; Abcam), goat anti-rabbit (1:500 dilution, cat no. ab7090; Abcam), or goat anti-rat (1:500 dilution, cat no. ab97057; Abcam) antibodies. After washing with TBS-T buffer, proteins were detected using ECL reagent (GE Healthcare Life Sciences). Gray values were quantified with ImageJ software.

### Quantitative RT-PCR

Total mRNA was extracted with TRIzol Reagent and the PureLink RNA Mini Kit (Life Technologies). RNA quality and concentration were checked by electrophoresis on 1.5% agarose gel and spectrophotometric analysis, respectively. Quantitative RT-PCR was performed with the High-Capacity cDNA Reverse Transcription Kits (Applied Biosystems/Life Technologies, Foster City, CA, USA). Samples were run in triplicate in an AB StepOne

Real Time PCR (Applied Biosystems) with TaqMan Gene Expression Master Mix (Applied Biosystems) using the following primers: Mm00440578m1 (P2X7R), Mm00840904m1 (NLRP3), Mm00445747g1 (ASC), and 4352339E (mouse glyceraldehyde 3-phosphate dehydrogenase, mGAPDH) (Applied Biosystems Life Technologies). Quantitative RT-PCR was performed in duplicate following Minimum Information for Publication of Quantitative Real-Time PCR Experiments guidelines (15).

### P2X7-GFP and Fura-2/AM imaging

The cytosolic  $\text{Ca}^{2+}$  concentration was measured using the fluorescent  $\text{Ca}^{2+}$  indicator Fura-2/AM (Life Technologies). HEK293-P2X7-GFP cells were grown on 24-mm coverslips and incubated at 37°C for 30 minutes in 1 mM  $\text{Ca}^{2+}$ -containing Krebs Ringer phosphate buffer supplemented with 2.5  $\mu\text{M}$  Fura-2/AM, 0.02% Pluronic F-68 (Sigma-Aldrich) and 0.1 mM sulfinpyrazone (Sigma-Aldrich). Cells were then rinsed and resuspended in 1 mM  $\text{Ca}^{2+}$ -containing Krebs Ringer phosphate. For  $\text{Ca}^{2+}$  measurements, cells were placed in an open Leyden chamber on a 37°C thermostated microscopy stage and imaged with an Olympus Xcellence microscopy system (Olympus, Shinjuku, Tokyo, Japan). Excitation filters 340/26 and 380/11 nm were used for Fura-2/AM and 485/20 nm for GFP (Chroma, Bellows Falls, VT, USA). Emission filter was 500/10 for both fura-2 and GFP imaging. Images were acquired with a Hamamatsu Orca R2 camera (Hamamatsu Photonics, Hamamatsu, Japan) using an exposure time of 20 ms, with a 500 ms delay per cycle. Microinjections were performed using an Eppendorf transjector 5246 microinjector system (Eppendorf, Hamburg, Germany). Stimuli were loaded into Eppendorf femtotips (Eppendorf) placed closer than 1  $\mu\text{m}$  to the cell edge. Single puffs (150 mM saline solution or 100  $\mu\text{M}$  BzATP dissolved in the same solution) were generated by applying a 200 hPa pressure pulse for 0.5 s. Control experiments were performed with the selective P2X7R antagonist AZ10606120 (300 nM; Tocris Bioscience, Bristol, UK). Fura-2/AM and P2X7R-GFP fluorescence emission (expressed as relative fluorescence units) was measured in the proximity of the site of stimulation and in an area distal to the stimulation site.

### Statistics

Data are expressed as mean  $\pm$  SEM, where  $n$  indicates the number of independent experiments. Statistical analysis was performed using the Student  $t$  test or the Mann-Whitney rank-sum test using Graphpad InStat (GraphPad Software, La Jolla, CA, USA).

## RESULTS

### P2X7R expression modulates NLRP3 levels

The P2X7R is not an integral constituent of the NLRP3 inflammasome; nonetheless, NLRP3 is required to drive P2X7R-dependent pro-IL-1 $\beta$  processing (16), and in addition, many NLRP3 stimulants act *via* P2X7R (6). To verify whether P2X7R expression and activity might modulate NLRP3 levels and, vice versa, NLRP3 expression and activity might modulate P2X7R levels, we selectively activated the P2X7R with ATP or its pharmacologic analog BzATP or stimulated NLRP3 with LPS. We initially used N13 mouse microglial cells as a model, which is a cell line widely used to investigate purinergic signaling and IL-1 $\beta$  maturation and release. N13 cells are available as the N13wt, characterized by high P2X7R expression, and the ATP-resistant (N13ATPR) variant, characterized by reduced P2X7R

expression, and are therefore useful to investigate P2X7R-dependent responses. As shown in **Fig. 1A, B**, ATP stimulation enhanced P2X7R and NLRP3 mRNA accumulation. A statistically significant ATP-stimulated increase in P2X7R mRNA occurred as early as 15 minutes, whereas a statistically significant increase in NLRP3 levels only occurred 60 min after P2X7R stimulation. BzATP had a similar effect, except that the NLRP3 mRNA increase was already detected at 30 min (**Fig. 1C, D**). Microglia challenge with LPS had no effect on P2X7R mRNA accumulation (**Fig. 1C**) but caused a large increase in NLRP3 mRNA levels (**Fig. 1D**). ASC mRNA accumulation did not change in response to either BzATP or LPS (**Fig. 1E**). Expression of the P2X7R protein was not affected by either LPS or BzATP treatment (**Fig. 1F**), whereas NLRP3 expression was up-modulated by LPS (**Fig. 1G**). ASC expression was increased by LPS or BzATP but not in a statistically significant fashion (**Fig. 1H**). A representative Western blot from control (CTR), LPS, or BzATP-stimulated N13 cells is shown in **Fig. 1I**.

**Fig. 1** shows that P2X7R stimulation, by ATP or BzATP, increases NLRP3 expression and suggests that NLRP3 levels might be up-modulated by P2X7R expression. To test this hypothesis, we took advantage of the N13ATPR cells selected for low P2X7R expression (11). The N13ATPR cells express P2X7R mRNA and protein to a level of  $\sim$ 50% and 25% that of the N13wt population, respectively (**Fig. 2A, B**). NLRP3 mRNA content of N13ATPR was almost 8-fold higher than that of N13wt, but this striking increase in mRNA content did not translate into an increased protein level. In fact, NLRP3 protein in N13ATPR was  $\sim$ 30% that of WT cells (**Fig. 2C, D**). ASC mRNA showed little change, whereas ASC protein in N13ATPR was  $\sim$ 30% that of N13wt cells (**Fig. 2E, F**). A representative blot of NLRP3, P2X7R, and ASC protein expression in N13wt and N13ATPR cells is shown in **Fig. 2G**. Western blot data were confirmed by immunofluorescence, which showed a striking reduction of both P2X7R and NLRP3 labeling in N13ATPR cells (**Fig. 1H**). These findings suggested P2X7R expression modulates NLRP3 expression levels.

To verify whether NLRP3 modulation by P2X7R expression is a general finding, we extended the investigation to additional mouse cell models that natively express both P2X7R and NLRP3 at a high level: primary peritoneal macrophages and primary microglial cells from C57Bl/6 WT and P2X7 $^{-/-}$  mice and P2X7R-silenced B16 mouse melanoma cells. **Fig. 3A, B** shows that, as expected, P2X7R mRNA and protein were fully absent in peritoneal macrophages from P2X7R $^{-/-}$  mice. NLRP3 mRNA was increased (**Fig. 3C**), but contrary to N13ATPR, NLRP3 protein was  $\sim$ 2-fold higher than in WT mice, albeit the increase was not statistically significant ( $P = 0.6$ ; **Fig. 3D**). ASC mRNA and protein showed no changes (**Fig. 3E, F**). Western blot of macrophage proteins and immunofluorescence pictures are shown in **Fig. 3G, H**). A marked increase in NLRP3 mRNA and protein was also observed in P2X7 $^{-/-}$  microglia (**Fig. 3I-K**). In P2X7 $^{-/-}$  microglia, the increase in NLRP3 levels was clear cut and statistically significant compared with WT microglia, thus supporting the finding in P2X7 $^{-/-}$  macrophages shown in **Fig. 3D**. These experiments show that in genetically deleted animals, the absence of P2X7R increased NLRP3 mRNA and NLRP3

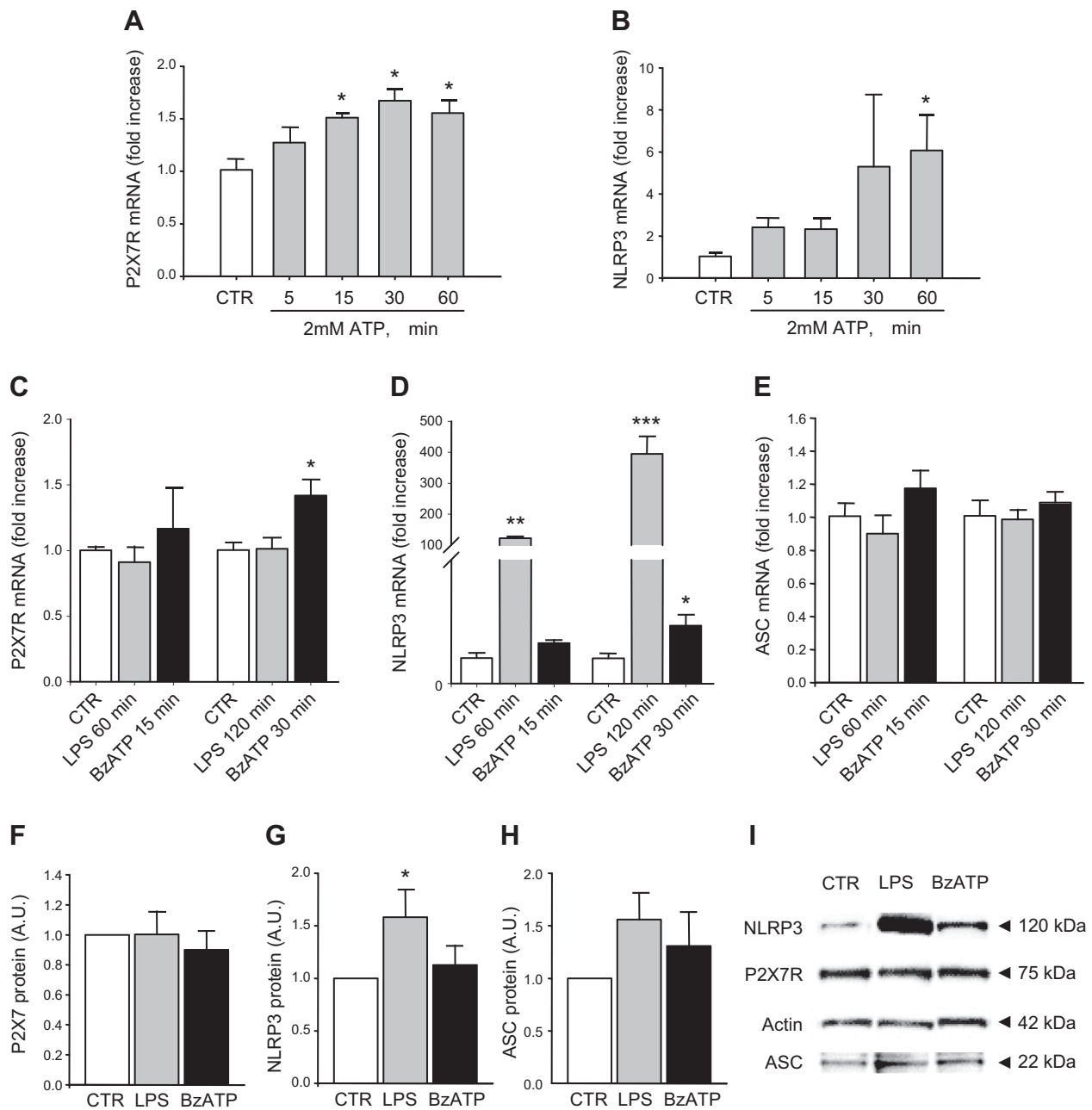


**Figure 1.** Purinergic and TLR4 agonists modulate P2X7R and NLRP3 expression. *A, B*) Time course of ATP-stimulated P2X7R and NLRP3 mRNA accumulation in N13 microglia, normalized over GAPDH mRNA levels, and expressed as fold increase over controls (CTR,  $n = 3$ ). *C–E*) LPS- or BzATP-stimulated accumulation of P2X7R (*C*), NLRP3 (*D*), and ASC (*E*) mRNA normalized over GAPDH mRNA levels and expressed as fold increase over controls ( $n = 3$ ). *F–H*) Densitometric analysis of P2X7R (*F*), NLRP3 (*G*), and ASC (*H*) protein in response to LPS or BzATP expressed as a fold increase over controls ( $n = 3$ ). P2X7R, NLRP3, and ASC bands were normalized over the actin band. (*I*) Exemplificative Western blot showing P2X7R, NLRP3, and ASC accumulation in nonstimulated (CTR) and LPS- or BzATP-stimulated cells. Actin shown as loading control. Data are represented as mean  $\pm$  SEM. \* $P < 0.05$ ; \*\* $P < 0.01$ ; \*\*\* $P < 0.001$ .

protein. We also investigated the B16 melanoma cell model. In B16 cells, both P2X7R mRNA and protein were reduced by shRNA transfection to  $\sim 50\%$  of control levels, causing in parallel a marked increase of NLRP3 and ASC mRNA and a decrease of NLRP3 protein, whereas ASC protein was unchanged (data not shown). Although P2X7R down-modulation was achieved in N13ATPR microglia and B16 melanoma cells by different means, the end result was the same, *i.e.*, a decrease in P2X7R

expression caused a large increase in NLRP3 mRNA. However, at variance with macrophage and microglia from the P2X7R<sup>-/-</sup> mouse, the increase in NLRP3 mRNA did not translate into an increase in NLRP3 protein.

#### P2X7R and NLRP3 colocalize

Data shown in Figs. 1–3 suggested that P2X7R and NLRP3 might colocalize and interact. A more detailed

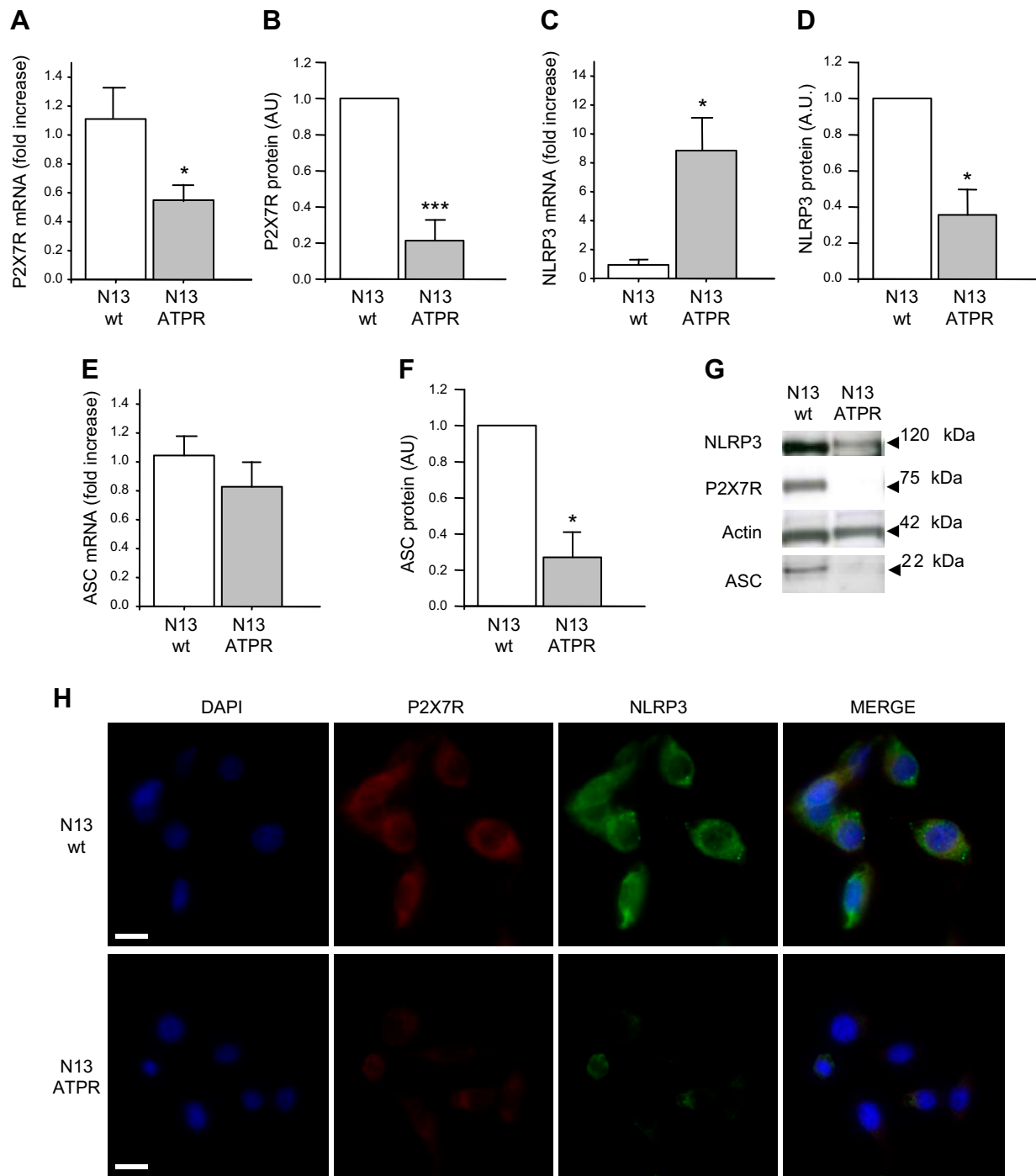


**Figure 2.** ATPR N13 cells express high NLRP3 mRNA and low NLRP3 protein levels. *A–D*) P2X7R and NLRP3 mRNA ( $n = 5$ ) and protein ( $n = 3$ ) levels in wild-type (N13wt) and ATP-resistant (N13ATPR) N13 microglia. *E, F*) ASC mRNA and protein levels in N13wt and N13ATPR microglia ( $n \geq 3$ ). P2X7R, NLRP3, and ASC mRNA levels of N13ATPR cells are expressed as fold change of N13wt normalized vs. GAPDH mRNA levels, whereas P2X7R, NLRP3, and ASC protein levels were normalized over actin levels and expressed as fold change of N13wt. *G*) Representative blot of P2X7R, NLRP3, and ASC expression in N13wt and N13ATPR microglia. Actin shown as loading control. *H*) Immunofluorescence labeling of P2X7R and NLRP3 proteins in N13wt and N13ATPR cells. Cells were stained with DAPI (blue) and immunolabeled with anti-P2X7R (red) and anti-NLRP3Abs (green). Merge, fourth column. Bar = 10  $\mu$ m. Data are represented as mean  $\pm$  SEM. \* $P < 0.05$ ; \*\*\* $P < 0.001$ .

confocal microscopy analysis indeed showed that P2X7R and NLRP3 did colocalize in N13wt cells (**Fig. 4A–D**). P2X7R and NLRP3 fluorescence distribution was analyzed at the single cell level by acquiring the fluorescence intensity profile across a single focal plan,

as shown in Fig. 4A, B. In addition, an orthogonal reconstruction of a Z-stack (7 planes; width pass, 0.8  $\mu$ m) was performed to highlight sites of enhanced P2X7R and NLRP3 colocalization (Fig. 4C, D). P2X7R showed a strong cytoplasmic and subplasmalemmal localization,

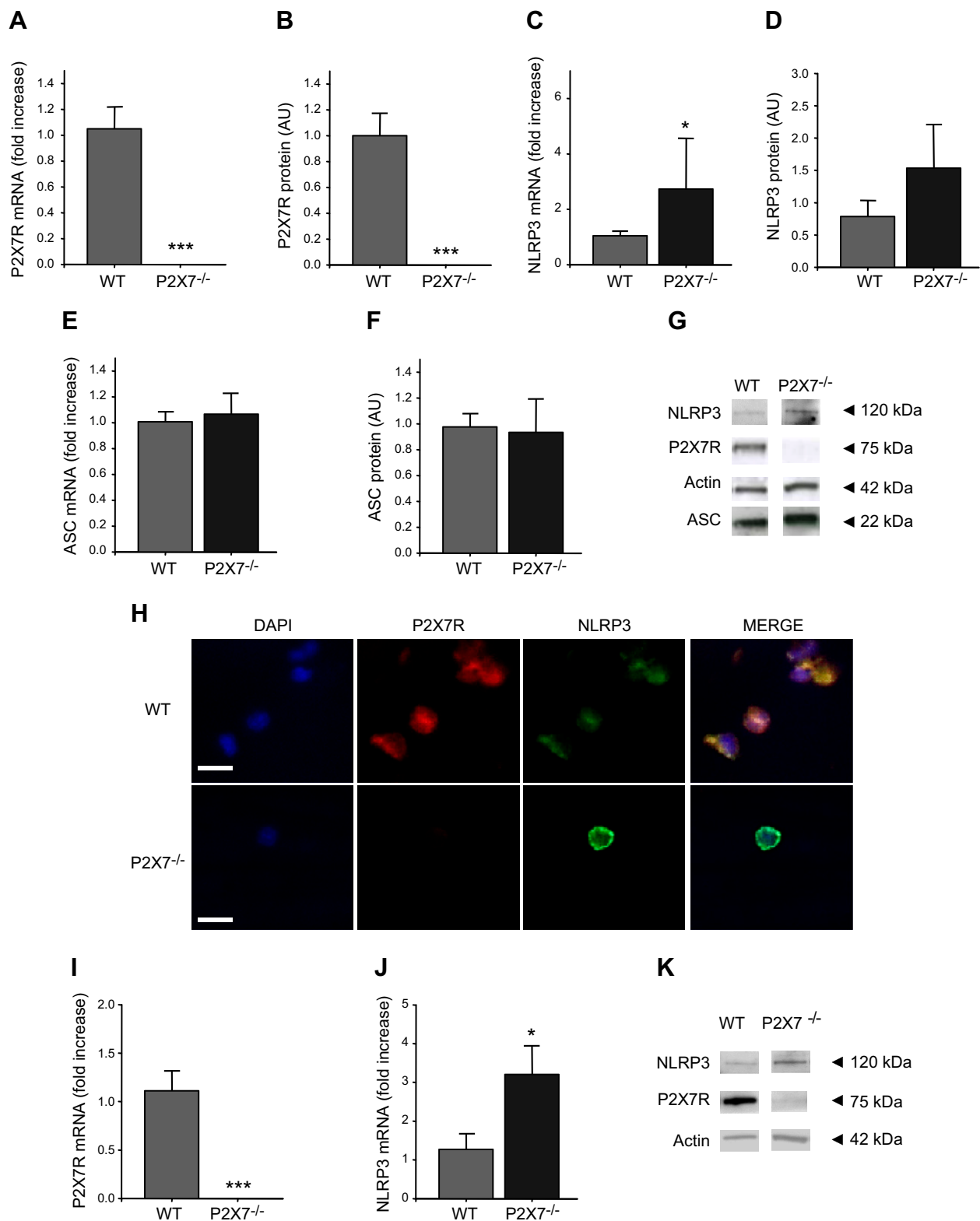


**Figure 3.** NLRP3 is up-regulated in macrophages and microglia from P2X7<sup>-/-</sup> mice. *A, B*) P2X7R expression in peritoneal macrophages from WT and P2X7<sup>-/-</sup> mice ( $n = 4$ ). *C, D*) NLRP3 expression in peritoneal macrophages from WT and P2X7<sup>-/-</sup> mice ( $n = 4$ ). *E, F*) ASC expression in peritoneal macrophages from WT and P2X7<sup>-/-</sup> mice ( $n = 4$ ). *G*) Representative Western blot of NLRP3, P2X7R, and ASC proteins from peritoneal macrophages from WT and P2X7<sup>-/-</sup> mice; actin is shown as loading control. *H*) Immunofluorescence labeling with anti-P2X7R (red) and anti-NLRP3 (green) of peritoneal macrophages from WT and P2X7<sup>-/-</sup> mice. Nuclei were stained with DAPI (blue). Merge, fourth column. *I, J*) P2X7R and NLRP3 mRNA expression in microglia from WT and P2X7<sup>-/-</sup> mice ( $n = 3$ ). *K*) Representative Western blot showing P2X7R and NLRP3 expression in microglia from WT and P2X7<sup>-/-</sup> mice; actin is shown as a loading control. All mRNA determinations are expressed as fold increase over WT samples and normalized vs. GAPDH mRNA levels. Protein levels were quantified by densitometry and normalized over actin protein content. Data are represented as mean  $\pm$  SEM. \* $P < 0.05$ ; \*\*\* $P < 0.001$ . Bar = 10  $\mu$ m.

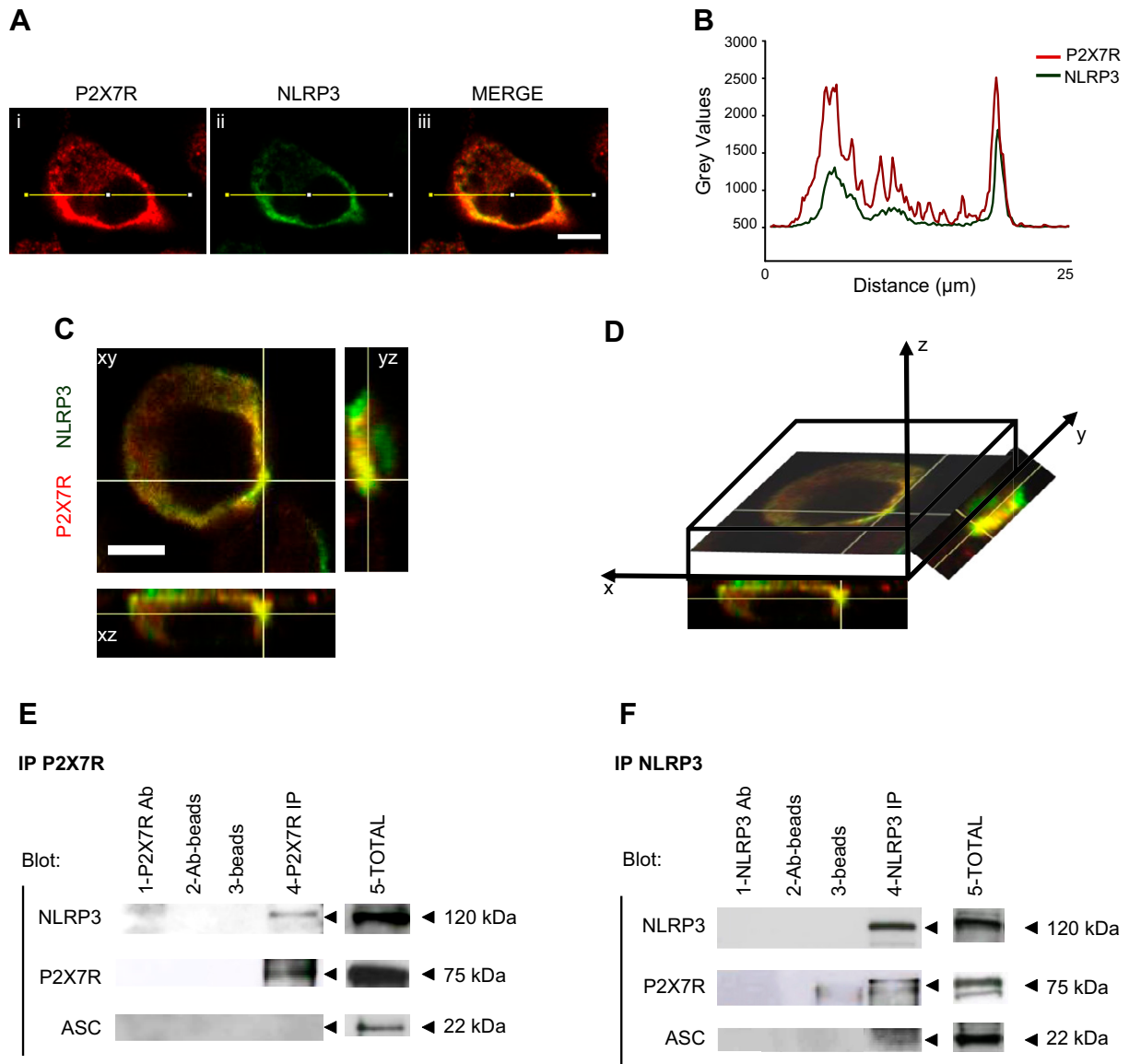


**Figure 4.** P2X7R and NLRP3 colocalize and closely interact. *A, B*) Microglial cells (1 of 20 analyzed is shown) were fixed and stained for P2X7R and NLRP3 as described in Materials and Methods, and then the fluorescence profile was run across the  $x$ - $y$  axes of the cell body (yellow line) at a focal plan set at  $3 \mu\text{m}$  and shown as intensity profile. *C, D*) 3D reconstruction of merged images obtained with confocal Z-stack (7 planes,  $0.8 \mu\text{m}$  step width) shown in orthogonal view. *E*) P2X7R immunoprecipitation ( $n = 3$ ). Lane 1, anti-P2X7R Ab in the absence of cell lysate; lane 2, eluate from Ab-coated beads in the absence of cell lysate; lane 3, eluate from Ab-uncoated beads incubated together with the cell lysate; lane 4, immunoprecipitate; lane 5, whole cell lysate. *F*) NLRP3 immunoprecipitation ( $n = 3$ ). Lane 1, anti-NLRP3 Ab in the absence of cell lysate; lane 2, eluate from Ab-coated beads in the absence of cell lysate; lane 3, eluate from Ab-uncoated beads incubated together with the cell lysate; lane 4, immunoprecipitate; lane 5, whole cell lysate. Scale bar,  $5 \mu\text{m}$ .

whereas the plasma membrane signal was rather weak (Fig. 4*A, B*). NLRP3 was also localized within the cytoplasmic and the subplasmalemmal regions (Fig. 4*B*). The nucleus was largely negative for both P2X7R and NLRP3. The 3D orthogonal reconstruction shown in Fig. 4*C* revealed “hot spots,” 1 or 2 per cell, close to the plasma membrane, where P2X7R and NLRP3 colocalized.

P2X7R/NLRP3 interaction was further investigated by immunoprecipitation. Fig. 4*E, F* shows that NLRP3 was immunoprecipitated together with P2X7R, and reciprocally, P2X7R was immunoprecipitated together

with NLRP3. ASC was also found in the immunoprecipitated complexes.

Next, we analyzed the single cell fluorescence profile and the Z-stack of individual LPS- or BzATP-treated cells. Fig. 5*A–D* shows that LPS or BzATP stimulation caused a slight increase in the expression of both P2X7R and NLRP3 and a shift of fluorescence from the cell body to the periphery. Z-stack analysis showed a single hot spot of increased P2X7R/NLRP3 interaction near the plasma membrane (Fig. 5*E, F*). Effect of BzATP or LPS stimulation on the P2X7R/NLRP3 interaction was also analyzed by coimmunoprecipitation experiments (Fig. 5*G,*

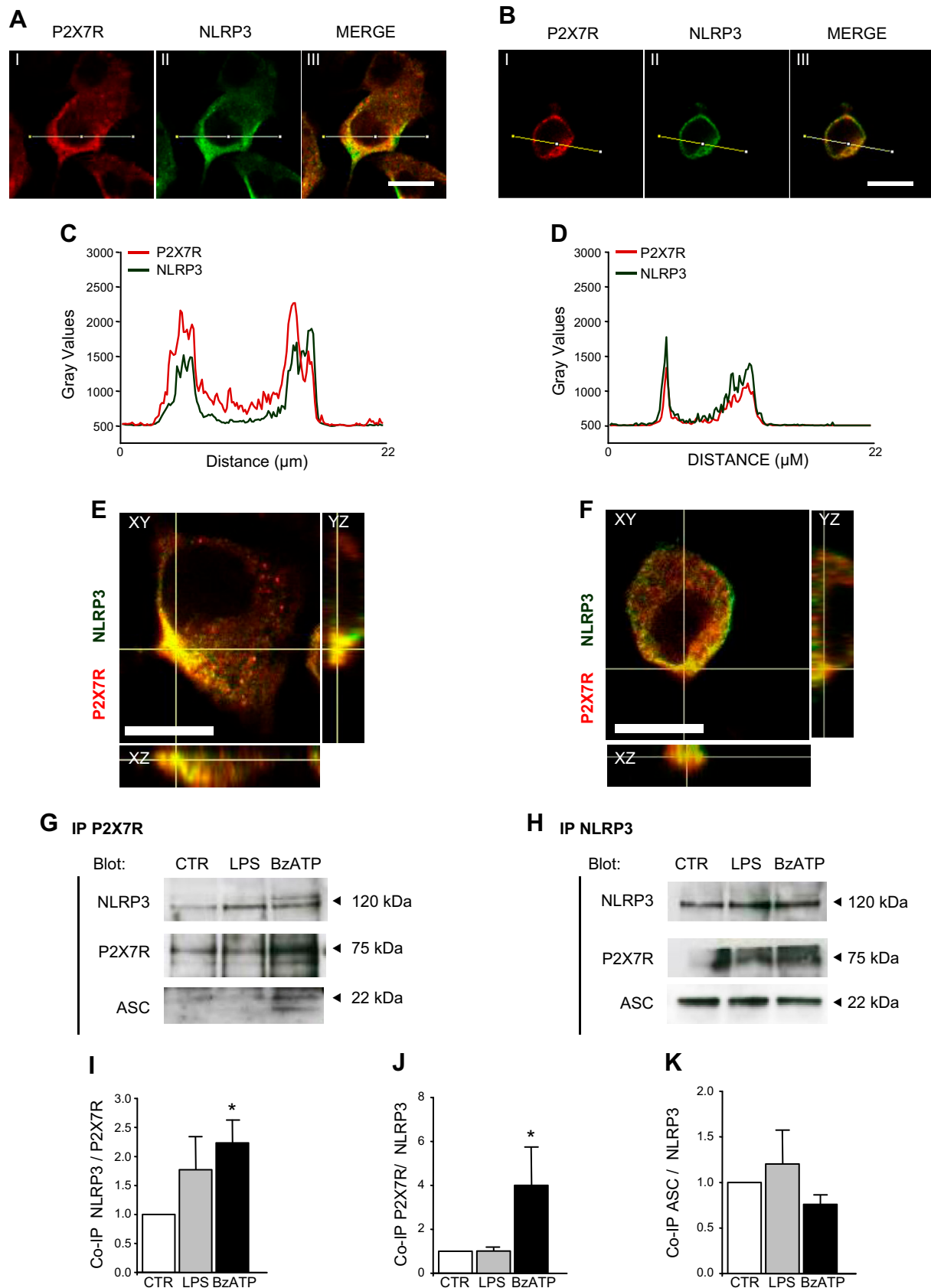


**Figure 5.** Stimulation with BzATP or LPS increases P2X7R/NLRP3 colocalization. *A–F*) Microglial cells were stimulated with either LPS (1  $\mu\text{g}/\text{ml}$ , 2 h, *A, C, E*), or BzATP (300  $\mu\text{M}$ , 30 min, *B, D, F*), fixed, and stained as described in Materials and Methods, and then the fluorescence profile was run across the *x-y* axes (yellow line) of the cell body at a focal plan set at 3  $\mu\text{m}$ . 3D (continued on next page)



H). Stimulation with BzATP significantly increased the amount of P2X7R or NLRP3 protein found in the complex, irrespective of whether anti-P2X7R or anti-NLRP3 antibodies were used for immunoprecipitation (Fig. 5I, J). On the contrary, BzATP or LPS treatment did not increase the content of ASC protein in the anti-NLRP3 antibody-immunoprecipitated samples (Fig. 5H, K), whereas in BzATP-treated cells, ASC protein was mostly detectable in P2X7R immunoprecipitated samples (Fig. 5G).

The P2X7R has a major role in the activation of NLRP3 in immune cells because this receptor is the main effector of the drop in cytosolic  $K^+$  that is generally thought to be the main trigger of NLRP3 inflammasome activation. However, it is reasonable to assume that changes in the  $K^+$  cytoplasmic concentration are spatially restricted to avoid a generalized, potentially deadly, depletion of intracellular  $K^+$ . Thus, we hypothesized that the colocalization of P2X7R and NLRP3 might be functional to restrict P2X7R-dependent ion changes at discrete sites of the subplasmalemmal cytoplasm, where inflammasome activation could be maximized. As a model to test this hypothesis, we used HEK293 cells stably transfected with a GFP-tagged P2X7R (HEK293-P2X7R-GFP), and, because of the lack of suitable indicators of intracellular  $K^+$ , the cytoplasmic  $Ca^{2+}$  indicator Fura-2 as a sensor of local changes in the ion concentration. As shown in Fig. 6, a BzATP puff applied with a patch pipette caused a rapid increase in the cytoplasmic  $Ca^{2+}$  concentration in the region under the pipette tip (Fig. 6C) but not in the distal cytoplasm (Fig. 6D). This fast  $Ca^{2+}$  rise was followed within several seconds by recruitment of additional P2X7Rs to the site of stimulation (Supplemental Movies S1 and S2). P2X7R was not recruited at sites distal to the point of application of BzATP, where no  $Ca^{2+}$  increase occurred (Fig. 6D). The  $Ca^{2+}$  increase and the associated P2X7R recruitment were specifically dependent on P2X7R activation, as shown by lack of a  $Ca^{2+}$  increase and of P2X7R recruitment in the presence of the highly selective P2X7R blocker AZ10606120 (Supplemental Fig. S1).

## DISCUSSION

Inflammasomes are multiprotein complexes responsible for the proteolytic conversion of procaspase-1 into caspase-1 and therefore for the conversion of pro-IL-1 $\beta$  and pro-IL-18 into the respective mature forms (2, 3). A thorough understanding of the molecular mechanism of activation is of fundamental importance in the context of inflammation. Thus far, 10 different inflammasome subtypes have been identified and classified according to the scaffold molecule (6). Among the different inflammasome subtypes, the NLRP3 inflammasome has a prominent status because of its involvement in autoinflammatory

diseases and its participation in many chronic inflammatory disorders (17). Several triggers for the NLRP3 inflammasome have been identified: cytoplasmic release of cathepsin B, the PKR kinase, thioredoxin inhibitory protein, cell swelling, an increase in the intracellular  $Ca^{2+}$  concentration, and efflux of cytosolic  $K^+$  (18–21). One of the most potent stimuli for NLRP3 inflammasome activation is extracellular ATP (10, 16).

Extracellular ATP is a ubiquitous DAMP acting at plasma membrane P2 receptors (22). The P2 receptor family is comprised of the P2Y and P2X subfamilies, numbering 8 and 7 members each (23). Within the P2 receptors, the only member associated with NLRP3 inflammasome activation is P2X7R (6), an ATP-gated cation selective channel that, on sustained stimulation, triggers the opening of a large conductance pore that mediates massive  $K^+$  efflux and  $Na^+$  and  $Ca^{2+}$  influx, as well as uptake of hydrophilic solutes of MW up to 900 Da (24). P2X7R and NLRP3 are obviously functionally linked given the prominent role of extracellular ATP as a DAMP and a stimulus for IL-1 $\beta$  maturation and release. In addition, present findings show that these 2 molecules are intimately linked, as P2X7R, besides inducing NLRP3 activation, also modulated NLRP3 expression levels. P2X7R down-modulation, whether induced by prolonged exposure to high extracellular ATP concentrations (N13ATPR cells), by shRNA (B16 melanoma cells) transfection, or by genetic deletion (P2X7 $^{-/-}$  macrophage and microglia cells), was always associated to a large increase in NLRP3 mRNA accumulation. However, at the protein level, induced vs. genetic P2X7R down-modulation had opposite effects: induced P2X7R down-modulation was paralleled by a decrease in NLRP3 protein expression, whereas on the contrary, genetic P2X7R deletion was associated to a striking increase in NLRP3 expression. ASC expression did not show a clear-cut pattern of changes in response to P2X7R down-modulation, because in N13ATPR cells, ASC protein was significantly reduced compared with N13wt, whereas in shRNA-treated B16 cells, despite a large increase in mRNA accumulation, it was unchanged. In cells from P2X7 $^{-/-}$  mice, neither ASC mRNA nor protein expression differed compared with WT. It needs to be stressed that the procedures used to acutely down-modulate P2X7R inevitably cause cell activation (because of sustained stimulation with extracellular ATP or to shRNA transfection), which despite increased mRNA accumulation, might accelerate NLRP3 protein degradation; thus, they are not directly comparable to genetic deletion.

A typical feature of the P2X7R is its ability to drive large transmembrane cation fluxes via a poorly characterized nonselective large conductance pore (9, 25). The physiologic significance of the large P2X7R pore is currently unknown. It has been hypothesized that it is involved in cytotoxicity (26), but although it is undisputed that under

---

reconstruction of LPS- (E) or BzATP-treated (F) cells obtained with confocal Z-stack (7 planes, 0.8  $\mu$ m step width) shown in orthogonal view. G, H) Coimmunoprecipitation of P2X7R and NLRP3 proteins in the absence or presence of LPS or BzATP, using an anti-P2X7R (G) or and anti-NLRP3 (H) immunoprecipitating antibody. I–K) Densitometry of immunoprecipitated NLRP3 normalized over P2X7R signal (I) ( $n = 4$ ), and P2X7R (J) ( $n = 4$ ) and ASC (K) ( $n = 4$ ) over NLRP3 signal. Data are represented as mean  $\pm$  SEM. \* $P < 0.05$ . Scale bar, 5  $\mu$ m.

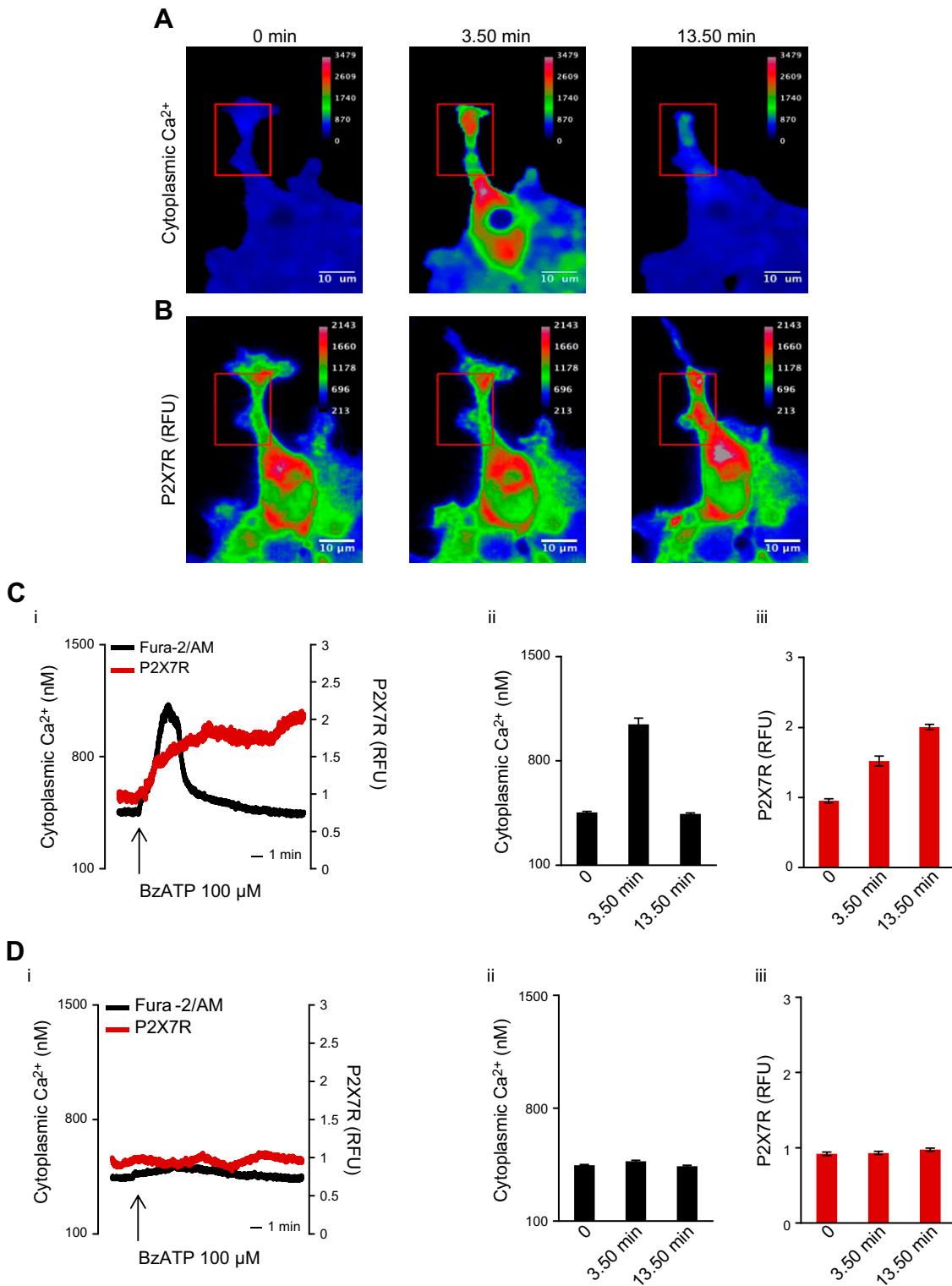


**Figure 6.** P2X7R activation drives P2X7R recruitment at discrete subplasmalemmal foci. HEK293 cells were transfected with rat P2X7R-GFP, as described in Materials and Methods, loaded with Fura-2/AM, placed in an open, thermostatted Leyden chamber at 37°C, and challenged with a BzATP puff (100 μM) delivered with an Eppendorf femtotip connected to an Eppendorf microinjector system (Materials and Methods). Images were acquired at the indicated time points as described in Materials and Methods. *A*) BzATP-triggered cytoplasmic Ca<sup>2+</sup> changes. *B*) BzATP-triggered P2X7R-GFP recruitment. *Ci–Ciii*) Kinetics and statistical analysis of BzATP-triggered cytoplasmic Ca<sup>2+</sup> changes and P2X7R-GFP recruitment measured in area within the red square shown in *A* and *B* (*n* = 10). *Di–Diii*) Kinetics and statistical analysis of BzATP-triggered cytoplasmic Ca<sup>2+</sup> changes and P2X7R-GFP recruitment measured at a cytoplasmic site distal to the site of stimulation (*n* = 10). Data are represented as mean ± SEM. Bar = 10 μm.

certain *in vitro* conditions P2X7R mediates necrotic or apoptotic cell death, it is also pretty clear that P2X7R functions are not restricted to cell death (27, 28). This is even more cogent as the role of P2X7R in inflammation and immunity increasingly appears to be important (29). The proinflammatory function of the P2X7R large pore might be easier to understand if its activation was restricted to localized cytoplasmic sites where the associated  $\text{Ca}^{2+}$  increase and  $\text{K}^+$  drop were sensed by an appropriate transduction system. The NLRP3 inflammasome is likely to be the chief transduction apparatus that converts the drop in cytosolic  $\text{K}^+$  caused by P2X7R receptor activation into a proinflammatory signal. Although P2X7R is not necessary for NLRP3 activation by certain stimuli that gain direct access to the cytoplasm (30, 31), it is now clear that  $\text{K}^+$  efflux is the common final pathway that drives NLRP3 inflammasome activation (7). Few, if any, plasma membrane receptors are able to trigger fast and massive  $\text{K}^+$  fluxes like P2X7R, and in turn, P2X7R-mediated inflammasome activation is entirely dependent on NLRP3 expression (16).

Present data suggest that, although the P2X7R is not an integral inflammasome component, it associates to the inflammasome at discrete foci in the subplasmalemmal region, in both resting and activated conditions. Close interaction between P2X7R and NLRP3 has important implications for the mechanism of inflammasome activation because it localizes NLRP3 exactly where the  $\text{K}^+$  drop occurs, maximizing NLRP3 stimulation and minimizing possible untoward effects caused by an unrestricted loss of cytoplasmic  $\text{K}^+$ . Furthermore, increased P2X7R/NLRP3 recruitment triggered by P2X7R stimulation provides a molecular mechanism for the amplification of the initial proinflammatory stimulus. Recruitment of P2X7R at discrete plasma membrane sites might be beneficial in additional ways, *e.g.*, to concentrate P2X7R where it is needed for inflammasome activation and to remove P2X7R from areas where its activation might cause an unnecessary and even detrimental perturbation of cytoplasmic ion homeostasis. Interestingly, P2X7R stimulation promoted P2X7R and NLRP3 colocalization but had a small effect on total cellular P2X7R or NLRP3 levels. On the contrary, LPS was an efficient stimulus for both colocalization and enhanced P2X7R and NLRP3 expression, both at the mRNA and protein level. In response to ATP, BzATP, or LPS, the adaptor molecule ASC showed little changes, whether at the mRNA or protein level.

In conclusion, we show that P2X7R and NLRP3 closely interact and colocalize at discrete sites in the subplasmalemmal cytoplasm where P2X7R-dependent changes in the ion concentration occur. This allows inflammasome activation and prevents possible cell damage caused by a generalized and uncontrolled increase in cytoplasmic  $\text{Ca}^{2+}$  and depletion of cytosolic  $\text{K}^+$ . Fj

F.D.V. is supported by Italian Association for Cancer Research Grant IG 5354, Telethon of Italy Grant GGP06070, an European Research Area Network Neuron Joint Transnational Project “Nanostroke” grant, Ministry of Health of Italy Grant RF-2011-02348435, Italian Ministry of Education, University and Research Grant RBAP11FXBC\_001, and institutional funds from the University of Ferrara. F.D.V. was

also supported by a grant from the Commission of European Communities (7th Framework Program HEALTH-F2-2007-202231 “ATPBone”). P.P. is supported by Italian Association for Cancer Research Grant IG 14442 and grants from the Italian Ministry of Education, University and Research (Progetti Ricerca Interesse Nazionale 20129JLHSY\_002, and RBAP11FXBC\_002, and Futuro in Ricerca RBFR10EGVP\_001).

## REFERENCES

- Martinon, F., Burns, K., and Tschopp, J. (2002) The inflammasome: a molecular platform triggering activation of inflammatory caspases and processing of proIL-beta. *Mol. Cell* **10**, 417–426
- Lamkanfi, M., and Dixit, V. M. (2014) Mechanisms and functions of inflammasomes. *Cell* **157**, 1013–1022
- Schroder, K., and Tschopp, J. (2010) The inflammasomes. *Cell* **140**, 821–832
- Davis, B. K., Wen, H., and Ting, J. P. (2011) The inflammasome NLRs in immunity, inflammation, and associated diseases. *Annu. Rev. Immunol.* **29**, 707–735
- Gross, O., Thomas, C. J., Guarda, G., and Tschopp, J. (2011) The inflammasome: an integrated view. *Immunol. Rev.* **243**, 136–151
- Di Virgilio, F. (2013) The therapeutic potential of modifying inflammasomes and NOD-like receptors. *Pharmacol. Rev.* **65**, 872–905
- Muñoz-Planillo, R., Kuffa, P., Martínez-Colón, G., Smith, B. L., Rajendiran, T. M., and Núñez, G. (2013)  $\text{K}^+$  efflux is the common trigger of NLRP3 inflammasome activation by bacterial toxins and particulate matter. *Immunity* **38**, 1142–1153
- Di Virgilio, F., Chiozzi, P., Ferrari, D., Falzoni, S., Sanz, J. M., Morelli, A., Torboli, M., Bolognesi, G., and Baricordi, O. R. (2001) Nucleotide receptors: an emerging family of regulatory molecules in blood cells. *Blood* **97**, 587–600
- Pelegri, P., and Surprenant, A. (2006) Pannexin-1 mediates large pore formation and interleukin-1beta release by the ATP-gated P2X7 receptor. *EMBO J.* **25**, 5071–5082
- Di Virgilio, F. (2007) Liaisons dangereuses: P2X(7) and the inflammasome. *Trends Pharmacol. Sci.* **28**, 465–472
- Ferrari, D., Villalba, M., Chiozzi, P., Falzoni, S., Ricciardi-Castagnoli, P., and Di Virgilio, F. (1996) Mouse microglial cells express a plasma membrane pore gated by extracellular ATP. *J. Immunol.* **156**, 1531–1539
- Lemaire, I., Falzoni, S., Leduc, N., Zhang, B., Pellegatti, P., Adinolfi, E., Chiozzi, P., and Di Virgilio, F. (2006) Involvement of the purinergic P2X7 receptor in the formation of multinucleated giant cells. *J. Immunol.* **177**, 7257–7265
- Sanz, J. M., Chiozzi, P., Ferrari, D., Colaianna, M., Idzko, M., Falzoni, S., Fellin, R., Trabace, L., and Di Virgilio, F. (2009) Activation of microglia by amyloid beta requires P2X7 receptor expression. *J. Immunol.* **182**, 4378–4385
- Bolte, S., and Cordelières, F. P. (2006) A guided tour into subcellular colocalization analysis in light microscopy. *J. Microsc.* **224**, 213–232
- Huggett, J. F., Foy, C. A., Benes, V., Emslie, K., Garson, J. A., Haynes, R., Hellems, J., Kubista, M., Mueller, R. D., Nolan, T., Pfaffl, M. W., Shipley, G. L., Vandesompele, J., Wittwer, C. T., and Bustin, S. A. (2013) The digital MIQE guidelines: Minimum Information for Publication of Quantitative Digital PCR Experiments. *Clin. Chem.* **59**, 892–902
- Mariathasan, S., Weiss, D. S., Newton, K., McBride, J., O’Rourke, K., Roose-Girma, M., Lee, W. P., Weinrauch, Y., Monack, D. M., and Dixit, V. M. (2006) Cryopyrin activates the inflammasome in response to toxins and ATP. *Nature* **440**, 228–232
- Haneklaus, M., O’Neill, L. A., and Coll, R. C. (2013) Modulatory mechanisms controlling the NLRP3 inflammasome in inflammation: recent developments. *Curr. Opin. Immunol.* **25**, 40–45
- Hornung, V., Bauernfeind, F., Halle, A., Samstad, E. O., Kono, H., Rock, K. L., Fitzgerald, K. A., and Latz, E. (2008) Silica crystals and aluminum salts activate the NALP3 inflammasome through phagosomal destabilization. *Nat. Immunol.* **9**, 847–856

19. Lu, B., Nakamura, T., Inouye, K., Li, J., Tang, Y., Lundbäck, P., Valdes-Ferrer, S. I., Olofsson, P. S., Kalb, T., Roth, J., Zou, Y., Erlandsson-Harris, H., Yang, H., Ting, J. P., Wang, H., Andersson, U., Antoine, D. J., Chavan, S. S., Hotamisligil, G. S., and Tracey, K. J. (2012) Novel role of PKR in inflammasome activation and HMGB1 release. *Nature* **488**, 670–674
20. Zhou, R., Tardivel, A., Thorens, B., Choi, I., and Tschopp, J. (2010) Thioredoxin-interacting protein links oxidative stress to inflammasome activation. *Nat. Immunol.* **11**, 136–140
21. Latz, E., Xiao, T. S., and Stutz, A. (2013) Activation and regulation of the inflammasomes. *Nat. Rev. Immunol.* **13**, 397–411
22. Rayah, A., Kanellopoulos, J. M., and Di Virgilio, F. (2012) P2 receptors and immunity. *Microbes Infect.* **14**, 1254–1262
23. Burnstock, G. (2007) Physiology and pathophysiology of purinergic neurotransmission. *Physiol. Rev.* **87**, 659–797
24. Steinberg, T. H., Newman, A. S., Swanson, J. A., and Silverstein, S. C. (1987) ATP<sub>4</sub>-permeabilizes the plasma membrane of mouse macrophages to fluorescent dyes. *J. Biol. Chem.* **262**, 8884–8888
25. Surprenant, A., Rassendren, F., Kawashima, E., North, R. A., and Buell, G. (1996) The cytolytic P2Z receptor for extracellular ATP identified as a P2X receptor (P2X<sub>7</sub>). *Science* **272**, 735–738
26. Di Virgilio, F., Bronte, V., Collavo, D., and Zanovello, P. (1989) Responses of mouse lymphocytes to extracellular adenosine 5'-triphosphate (ATP). Lymphocytes with cytotoxic activity are resistant to the permeabilizing effects of ATP. *J. Immunol.* **143**, 1955–1960
27. Di Virgilio, F. (1995) The P2Z purinoceptor: an intriguing role in immunity, inflammation and cell death. *Immunol. Today* **16**, 524–528
28. Di Virgilio, F., Ferrari, D., and Adinolfi, E. (2009) P2X<sub>7</sub>: a growth-promoting receptor-implications for cancer. *Purinergic Signal.* **5**, 251–256
29. Bours, M. J., Dagnelie, P. C., Giuliani, A. L., Wesselius, A., Di Virgilio, F. (2011) P2 receptors and extracellular ATP: a novel homeostatic pathway in inflammation. *Front. Biosci. (Schol. Ed.)* **3**, 1443–1456
30. Franchi, L., Kanneganti, T. D., Dubyak, G. R., and Núñez, G. (2007) Differential requirement of P2X<sub>7</sub> receptor and intracellular K<sup>+</sup> for caspase-1 activation induced by intracellular and extracellular bacteria. *J. Biol. Chem.* **282**, 18810–18818
31. Harder, J., Franchi, L., Muñoz-Planillo, R., Park, J. H., Reimer, T., and Núñez, G. (2009) Activation of the Nlrp3 inflammasome by *Streptococcus pyogenes* requires streptolysin O and NF-κB activation but proceeds independently of TLR signaling and P2X<sub>7</sub> receptor. *J. Immunol.* **183**, 5823–5829

*Received for publication December 11, 2014.*

*Accepted for publication January 27, 2015.*